Current profile modification experiments in EXTRAP T2R

M Cecconello[1], J-A Malmberg[1], G Spizzo[2], B E Chapman[3], R M Gravestjin[4], P Franz[2,5], P Piovesan[2], P Martin[2] and J R Drake[1]

[1] Division of Fusion Plasma Physics (Association EURATOM/VR), Alfvén Laboratory, Royal Institute of Technology, SE 100 44, Stockholm, Sweden
[2] Consorzio RFX, Associazione EURATOM-ENEA sulla Fusione, Padova, Italy
[3] Department of Physics, University of Wisconsin-Madison, Madison, WI 53706, USA
[4] Department of Atomic and Molecular Physics, Royal Institute of Technology, SE 100 44, Stockholm, Sweden
[5] Istituto Nazionale di Fisica della Materia, Unità di Ricerca di Padova, Padova, Italy

Abstract

Pulsed poloidal current drive (PPCD) experiments have been conducted in the resistive shell EXTRAP T2R reversed-field pinch experiment. During the current profile modification phase, the fluctuation level of the $m = 1$ internally resonant tearing modes decreases, and the velocity of these modes increases. The $m = 0$ modes are not affected during PPCD, although termination occurs with a burst in the $m = 0$ amplitude. The PPCD phase is characterized by an increase in the central electron temperature (up to 380 eV) and in the soft x-ray signal. Spectroscopic observations confirm an increase in the central electron temperature. During PPCD, the plasma poloidal beta increases to 14%, and the estimated energy confinement time doubles, reaching 380 μs. The reduction in the fluctuation level and the corresponding increase in the energy confinement time are qualitatively consistent with a reduction in parallel transport along stochastic magnetic field lines.

1. Introduction

In a reversed-field pinch (RFP) fusion device the toroidal and poloidal magnetic fields have similar amplitudes, and the toroidal field at the edge and at the centre have opposite directions. As a result, this magnetic configuration is susceptible to a class of internally resonant tearing instabilities with poloidal mode number $m = 1$ and toroidal mode number $n \gtrsim 2R/a$, with R and a being the major and minor radii of the torus. These instabilities, driven by a gradient in the parallel current profile, generate a dynamo electric field that sustains the RFP configuration against resistive diffusion of the magnetic profiles. However, the overlapping of the magnetic islands, associated with the growth of these instabilities on their respective resonant surfaces,

results in a stochastic magnetic field structure in the plasma core. Parallel transport of particles and energy along stochastic magnetic field lines is a significant source of power loss and ultimately limits the confinement capability of an RFP.

A current profile modification technique known as pulsed poloidal current drive (PPCD) aims to reduce the parallel current gradient, suppress the internally resonant tearing instabilities and improve particle and energy confinement. This technique was originally performed in the Madison symmetric torus (MST) RFP, where a single fast pulse of current was driven in the toroidal field coils to generate a poloidal electric field at the plasma edge [1]. During PPCD, the fluctuation level decreased and the energy confinement time increased. This technique has been gradually improved in later experiments in MST [2–4] and has also been successfully applied in the RFX [5] and TPE-RX [6] RFP experiments.

In this paper we describe the first PPCD experiments performed in the EXTRAP T2R RFP [7]. EXTRAP T2R differs from MST, TPE-RX and RFX in that it is equipped with a resistive shell and has a large aspect ratio, R/a. PPCD experiments have been carried out in two different RFP equilibria characterized by initially weak and strong reversal of the edge toroidal magnetic field. The weak reversal equilibrium is characterized by a reversal parameter $F = B_\phi(a)/\langle B_\phi \rangle \approx -0.15$ and pinch parameter $\Theta = B_\theta(a)/\langle B_\phi \rangle \approx 1.6$. The strong reversal equilibrium is characterized by $F \approx -0.65$ and $\Theta \approx 2.1$. The results obtained show that the PPCD technique improves the plasma confinement properties also in an RFP with a resistive shell. The observed reduction in the magnetic fluctuations and the improvement in the energy confinement time are comparable with those reported in the first PPCD experiment in MST [1]. A significant improvement in the understanding of the dynamic behaviour of the relevant instabilities during PPCD has been possible due to a comprehensive set of magnetic diagnostics present in EXTRAP T2R that enables studies with a better mode spectral and temporal resolution than available in previous PPCD experiments. The mode dynamics during PPCD in EXTRAP T2R exhibits a number of features that include acceleration of the rotation of the internally resonant tearing $m = 1$ modes, change in the growth rate of the non-resonant resistive shell modes and the occurrence of an $m = 0$ burst at the end of PPCD.

The remainder of the paper is structured as follows: EXTRAP T2R, the experimental technique used to drive poloidal current at the edge and the diagnostics used in this study are described in section 2. Results of PPCD experiments with initially weak and strong reversal are presented and discussed in section 3. A summary of the paper is given in section 4.

2. Description of the experiment

EXTRAP T2R is a medium-sized RFP ($R/a = 1.24\,\text{m}/0.18\,\text{m} = 6.8$) characterized by a vertical magnetic field shell penetration time of $\approx 6.3\,\text{ms}$, with a plasma duration up to 25 ms. The first wall consists of a stainless steel vacuum vessel surrounded by a double copper shell. Protection of the first wall is provided by a set of molybdenum mushroom-shaped limiters that covers less than 8% of the total wall surface. The power supply system of EXTRAP T2R consists of three sets of capacitor banks. The first set (Ohmic heating circuit) consists of a three-stage bank and is used to inductively drive plasma current. These three stages are used for breakdown, current ramp-up and discharge sustainment. The second set (toroidal field circuit) also consists of a three-stage capacitor bank. The first bank is used to generate the initial toroidal field before breakdown. During the current ramp-up phase, the second bank (the fast reversal bank) is used to quickly reverse the toroidal field to bring the plasma to the desired equilibrium. The third bank is then used to set and sustain the reversal of the edge toroidal field. The third set (vertical field circuit) consists of a capacitor bank used to pre-set a magnetic vertical field for radial equilibrium control.

EXTRAP T2R is operated at plasma currents between 50 and 120 kA with a resistive toroidal loop voltage as low as 25 V. The electron density is in the range $(0.5–2.0) \times 10^{19} \, \text{m}^{-3}$ (without the use of a gas refuelling system to sustain the density during the discharge). In plasmas without PPCD, the central electron and ion temperatures range from 80 to 250 eV, poloidal beta varies between 5% and 15% and the energy confinement time varies between 50 and 250 μs. The internally resonant tearing modes rotate toroidally with typical angular phase velocities in the range -20 to -800 krad s^{-1} (the minus sign is used to indicate that these modes rotate in a direction opposite to the $m = 0$ modes). As a result, the tearing mode amplitudes are comparable with or even smaller than those observed in conducting shell experiments. On the other hand, the resistive shell modes do not rotate, and they grow on a timescale dependent on the plasma equilibrium but which is roughly of the order of the shell penetration time [8].

Operation of EXTRAP T2R for current profile modification experiments requires a different start-up procedure from that for standard scenarios. The fast reversal bank is not used during the current ramp-up phase: instead the plasma is allowed to self-reverse. This start-up scenario requires a lower initial toroidal field. Once the desired F is achieved, the fast reversal bank is fired to induce a single pulse of poloidal current (PPCD). The voltage on this bank can be varied to obtain different surface poloidal electric fields. This mode of operation has some limitations. In fact, the weak initial toroidal magnetic field sets an upper limit on the maximum strength of the vertical magnetic field that can be used to control the plasma radial equilibrium. Vertical fields stronger than this limit result in breakdown failure. As a result, radial equilibrium is not optimal and the plasma column is outwardly shifted by $\approx$2–3 mm ($\approx$2% of the minor radius). Consequently, PPCD discharges are sustained for times shorter than 12 ms to avoid damage to the first wall.

Standard diagnostics are used to measure the plasma current, I, the toroidal loop voltage, V_ϕ, and the reversal and pinch parameters F and Θ. The electron density profile, $n_e(r)$, is obtained by measuring, with a CO_2 interferometer, the line-integrated electron density along four different chords [9]. A surface barrier diode is used to monitor the soft x-ray (SXR) signal along a central line-of-sight. The central ion temperature is measured with a neutral particle energy analyser based on the time of flight technique [9]. The central electron temperature is measured with a single-shot, single-point Thomson scattering system [9]. The impurity content is monitored by a VUV spectrometer [10] equipped with a fast detection system that measures the temporal evolution of the impurity spectral emission in a wavelength region between 100 and 1100 Å. The instrument is absolutely calibrated using the branching ratio technique [11, 12]. In addition, several photomultiplier tubes with narrow bandwidth interference filters (FWHM $\approx$ 10 Å) record H$_\alpha$ emission at different poloidal and toroidal positions. A SXR photocamera equipped with 12 chords in a fan array [13] has been recently put into operation. The SXR photocamera photodiodes have a flat response from the visible to x-ray wavelength range. A curved beryllium absorber of 9 μm thickness, positioned between the photocamera pinhole and the diodes, is used to block SXR photons below 1 keV.

The magnetic diagnostics consist of three sets of pick-up coils placed between the vacuum vessel and the double-layered thin copper shell. They are used to measure the radial, poloidal and toroidal magnetic field components. For weakly reversed discharges, a set of 128 toroidal magnetic field coils at 4 poloidal $\times$ 32 toroidal positions is used to measure simultaneously the $m = 0$ and 1 components of the magnetic fluctuations up to a maximum toroidal mode number of $|n| = 15$. In this configuration, the helicity of the $m = 1$ modes can also be determined. In the convention used here, modes that have the same helicity as the equilibrium field inside the toroidal magnetic field reversal surface have $m = 1$, $n < 0$, while modes that have the same helicity as the equilibrium field outside the reversal surface have $m = 1$, $n > 0$. For strongly

reversed discharges, a set of pick-up coils measuring the toroidal magnetic field at 4 poloidal $\times$ 64 toroidal positions is used to analyse the $m = 1$ modes up to a maximum toroidal number of $|n| = 31$. In order to reduce the required amount of transient recorders for this configuration the coil signals are hardware subtracted directly, giving measurements of the $m = 1$ radial and vertical Fourier components. However, with this set-up, the $m = 0$ modes cannot be resolved.

3. Experimental observations

The PPCD campaign carried out in EXTRAP T2R has focused on two different target plasma equilibria that are characterized by initially weak or strong reversal. The weak reversal equilibrium discharges are typical of standard operation, while strong reversal operation is tested for the first time. The motivation for strong reversal is to combine the spontaneous improved confinement regimes with strong reversal observed in MST [4] with modification of the parallel current profile to test the possibility of further enhancing the confinement properties. Spontaneous improved confinement regimes at strong reversal were also observed in TPE-1RM20 [14].

Since PPCD experiments require self-reversed operation, a series of reference discharges without PPCD but employing self-reversal were also performed for the two different equilibria, thus allowing comparison between PPCD and non-PPCD conditions. In total, 290 discharges have been studied: 50 reference discharges for each equilibrium, 70 PPCD discharges at weak reversal and 120 PPCD discharges at strong reversal. The experimental observations for the weak and strong reversal scenarios are described separately in sections 3.1 and 3.2. The behaviour of the plasma impurities and the plasma confinement properties are described in sections 3.3 and 3.4, respectively, for both scenarios.

3.1. PPCD at weak reversal

The time traces of shot-averaged plasma parameters for weak reversal reference discharges are shown in figure 1. Reference discharges are characterized by F and Θ varying between -0.1 and -0.2, and 1.55 and 1.65, respectively. The plasma current is ramped up to $\approx 100\,\text{kA}$ and then decays slowly, as does the average toroidal flux. The line-averaged electron density decays throughout the discharge from 2×10^{19} to $0.5 \times 10^{19}\,\text{m}^{-3}$. The central electron and ion temperatures (not shown) are approximately constant during the discharge with values of $200\,\text{eV}$ and $170\,\text{eV}$, respectively. Figure 1 also shows the time evolution of the shot-averaged plasma quantities when PPCD is fired in reference discharges at 1.5 ms. The applied poloidal loop voltage results in a surface poloidal electric field that increases to $3\,\text{V}\,\text{m}^{-1}$ in less than 1 ms. PPCD causes a reduction in the average toroidal field and a decrease in the toroidal field at the edge. In particular, during PPCD the edge parallel electric field, $E_{\parallel}(a)$, is positive as required in order to avoid strong relaxation events. The equilibrium reaches an F and Θ value of -0.8 and 2.15, respectively. The line-averaged electron density also responds immediately to PPCD by remaining constant for 1 ms at $1.5 \times 10^{19}\,\text{m}^{-3}$. This has also been confirmed by the reconstruction of the electron density profile using measurements along four chords. No significant peaking of the electron density profile is observed during PPCD in comparison with reference discharges as shown in figure 2(*a*). The single-line-of-sight SXR signal shows a five-fold increase, reflecting an increment in the electron density and in the electron temperature. A comparison of the SXR emission profiles for PPCD and reference discharges, measured with the photocamera, is shown in figure 2(*b*). During PPCD the SXR signal increases in the whole plasma core. No significant change in SXR emissivity profile shape is observed. The electron
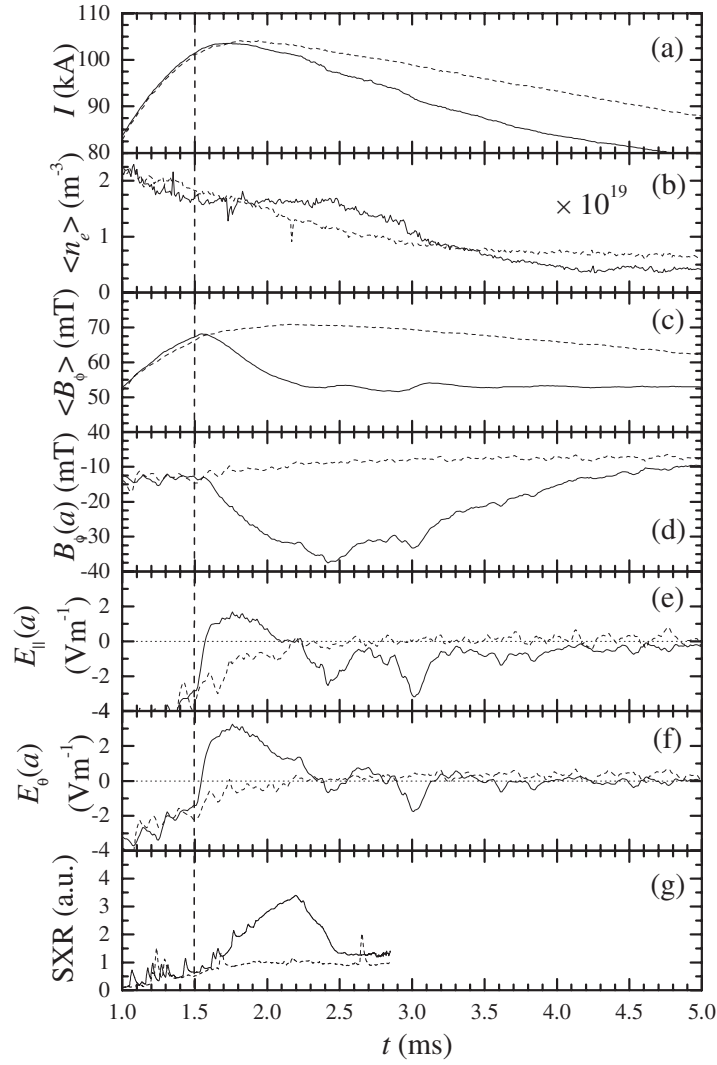
Figure 1. Time traces of plasma quantities for reference (- - - -) and PPCD (———) discharges at initially weak reversal. From top to bottom: (*a*) plasma current, (*b*) line-averaged electron density, (*c*) average toroidal magnetic field, (*d*) edge toroidal electric field, (*e*) surface parallel electric field, (*f*) surface poloidal electric field and (*g*) SXR signal. The vertical dashed line indicates the start of the PPCD.

temperature on axis has been measured directly with the Thomson scattering system at different times during PPCD, and it increases from 160 to 240 eV as shown in figure 3(*a*). The time evolution of the central ion temperature in PPCD discharges is quite different from that of reference discharges. The ion temperature does not change during PPCD (as also observed in [1, 4, 6]), and it is around 130 eV as shown in figure 3(*b*). However, at the end of the PPCD phase the ion temperature increases quite rapidly up to 240 eV and then decays to the pre-PPCD value on the same timescale required for the restoration of the equilibrium. The plasma current responds to PPCD by decaying faster than in reference discharges. The end of PPCD is brought about by the decay of the poloidal electric field, E_ϑ, ≈0.7 ms after the
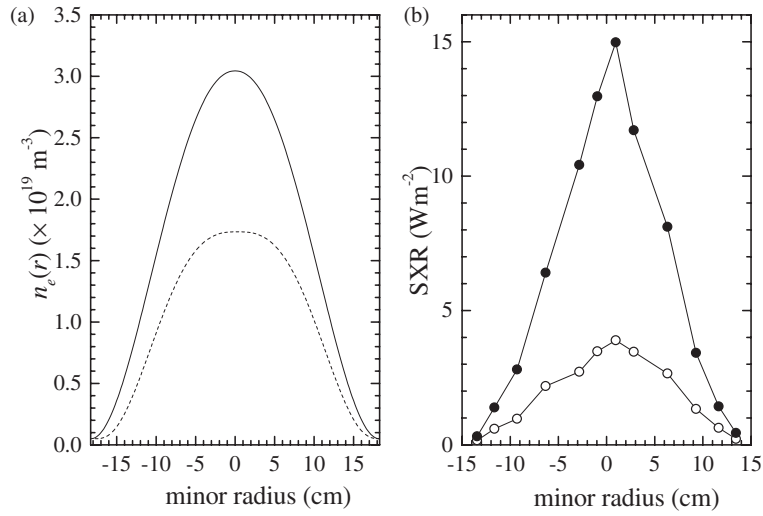
Figure 2. (*a*) Electron density profile for a reference (- - - -) and a PPCD (——) discharge at weak reversal at $t = 2.1$ ms; (*b*) SXR signal profile for a reference (○) and a PPCD (●) discharge at weak reversal observed with the photocamera at $t = 2.1$ ms.
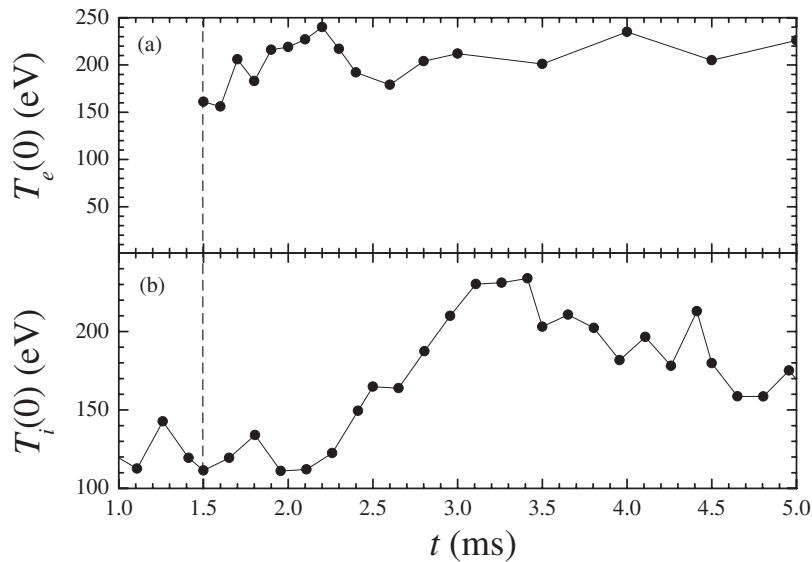

Figure 3. Time traces of (*a*) the central electron temperature and of (*b*) the central ion temperature for PPCD discharges at weak reversal. The vertical dashed line indicates the start of the PPCD.

start of the PPCD (see figure 1(*f*)). The plasma then reaches, in ≈3 ms, an equilibrium close to the initial one but characterized by a lower plasma current and toroidal flux. During this phase, the electron density decays faster compared with reference discharges as can be seen in figure 1(*b*).

Auxiliary current drive at weak reversal reduces the total fluctuation amplitude of the $m = 1$ modes as previously reported in other RFP experiments [3, 5, 6]. In figure 4(*a*) the
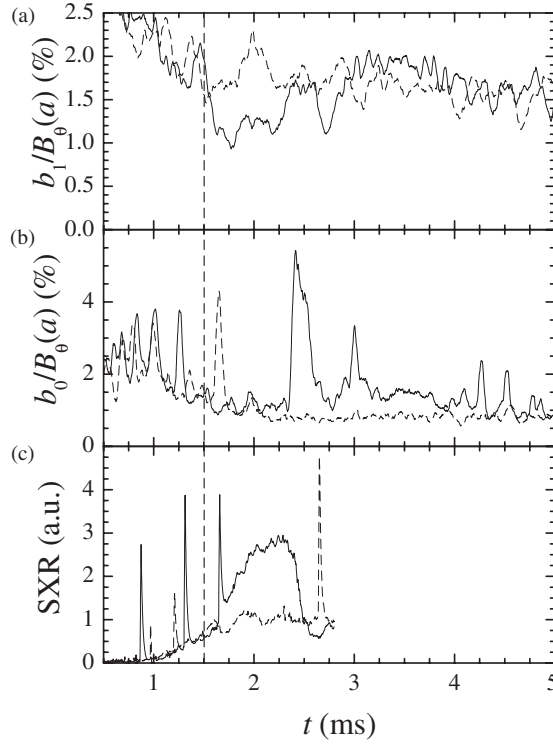
Figure 4. Time traces of a reference (- - - -) and of a PPCD (——) discharge. From top to bottom: (*a*) rms value of the $m = 1$, $n = -12$ to -15 modes, (*b*) rms value of the $m = 0$, $n = 1$–4 modes, (*c*) SXR signal. The vertical dashed line indicates the start of the PPCD.

root mean square (rms) values of the internally resonant tearing modes $m = 1$, $n = -12$ to -15 (normalized to the edge poloidal field) are plotted as a function of time for a reference and a PPCD discharge. The total fluctuation amplitude normalized to the edge poloidal magnetic field decreases from 1.5% to 1% at the same time that the SXR signal increases. While PPCD has an impact on the $m = 1$ fluctuation amplitude, it has only a weak influence on the $m = 0$ mode amplitude. This is shown in figure 4(*b*), where the rms of the $m = 0$, $n = 1$–4 modes is plotted as a function of time. The total $m = 0$ fluctuation amplitude during PPCD is similar to that of reference discharges, in contrast to the behaviour of the $m = 1$ modes. At the end of PPCD, the $m = 1$ fluctuations are restored to the pre-PPCD level and a burst in the $m = 0$ fluctuations takes place (see figure 4, $t \approx 2.4$ ms). This $m = 0$ burst is followed by a rapid decrease in the SXR emission and by an increase in the ion temperature as shown in figure 3(*b*).

During and after PPCD the angular phase velocity of the $m = 1$ tearing modes is greater (in absolute value) than during reference discharges as shown in figure 5(*b*). Since the $\boldsymbol{E} \times \boldsymbol{B}$ drift velocity (assuming an outwardly directed electric field due to ambipolar diffusion in a stochastic magnetic field) is proportional to the electron temperature, it is possible to assume that heating causes the plasma to rotate at a higher speed and to drag the $m = 1$ modes. However, it is not possible, at the present stage, to exclude other mechanisms (reduction of CX neutral momentum loss, for example) that might be responsible for the acceleration of the $m = 1$ tearing modes. The contribution to the phase velocity of the $m = 1$ tearing modes due to the diamagnetic term, proportional to pressure gradients, seems to be negligible since no significant peaking of the density profile and SXR emissivity profile are observed in
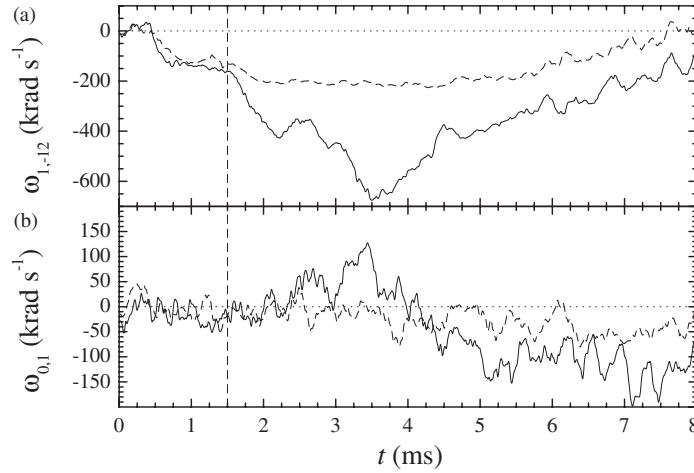
Figure 5. Time evolution of the angular phase velocities for the (*a*) $m = 1$ and the (*b*) $m = 0$ modes for discharges at weak reversal with (——) and without (- - - -) PPCD. The vertical dashed line indicates the start of the PPCD.
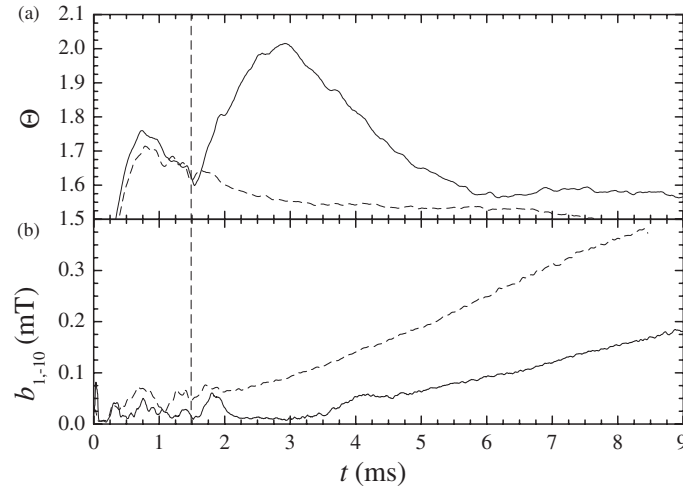

Figure 6. Time evolution of (*a*) the pinch parameter Θ and (*b*) of the internally non-resonant resistive wall mode $m = 1$, $n = -10$ for reference (- - - -) and PPCD (——) discharges. The vertical dashed line indicates the start of the PPCD.

PPCD discharges. At the end of PPCD and following the burst of the $m = 0$, $n = 1$ mode, the $m = 1$ tearing modes slow down significantly and then accelerate again when the amplitude of the $m = 0$, $n = 1$ mode decreases. It is interesting to note that the angular phase velocity of the $m = 0$, $n = 1$ mode is much smaller (in absolute value) than the angular phase velocity of the $m = 1$ modes and it oscillates between 0 and $100\,\mathrm{krad\,s^{-1}}$ as shown in figure 5(*b*). At the SXR crash the amplitude of the $m = 0$, $n = 1$ mode increases and so does its interaction with the $m = 1$ modes, which then slow down. At the same time a slight acceleration of the $m = 0$, $n = 1$ mode is observed.

An additional interesting feature of PPCD action can be observed in figure 6, where the time evolution of the internal $m = 1$, $n = -10$ non-resonant resistive shell mode is plotted for

a reference and a PPCD discharge together with the pinch parameter Θ. The growth rate of this internal resistive shell mode is clearly reduced by the strong equilibrium change produced by the application of PPCD. It is important to stress, however, that it is the change in the plasma equilibrium towards strongly reversed discharges (higher Θ) that causes the observed reduction in the growth rate of the internal non-resonant resistive shell mode. This has been predicted by linear MHD simulations [15] and experimentally observed in EXTRAP T2R [16].

3.2. PPCD at strong reversal

The time traces of shot-averaged plasma global parameters for strong reversal reference and PPCD discharges are shown in figure 7. The reference discharges are characterized by F and Θ
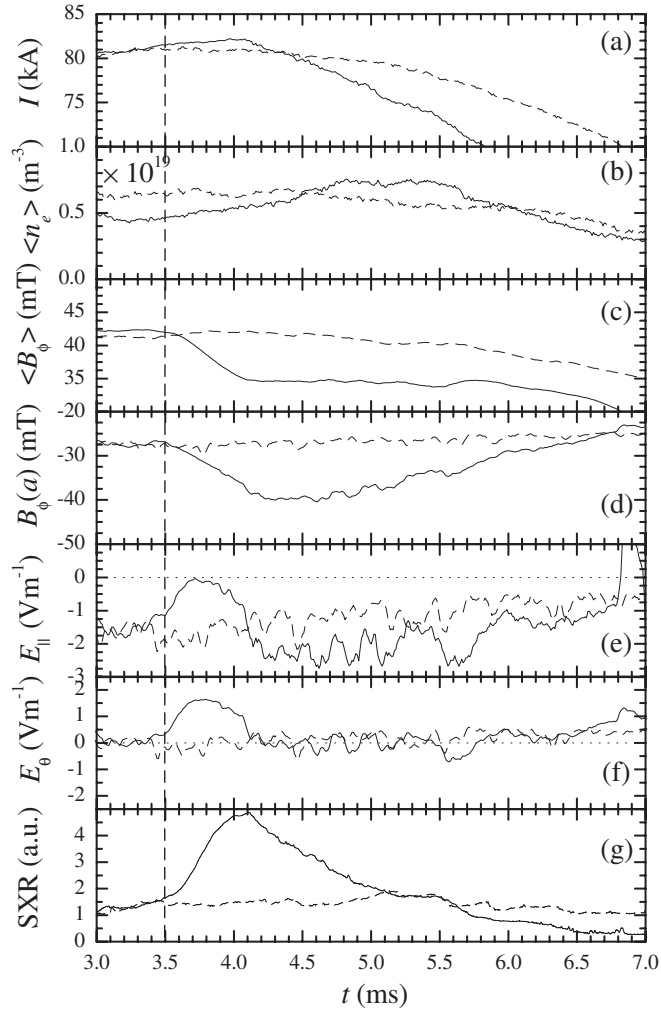

Figure 7. Time traces of plasma quantities for reference (- - - -) and PPCD (——) discharges at weak reversal. From top to bottom: (*a*) plasma current, (*b*) line-averaged electron density, (*c*) average toroidal magnetic field, (*d*) edge toroidal electric field, (*e*) surface parallel electric field, (*f*) surface poloidal electric field and (*g*) SXR signal. The vertical dashed line indicates the start of the PPCD.

in the ranges between -0.6 and -0.7, and 2.05 and 2.15, respectively. The plasma current is ramped up to ≈ 80 kA and then decays slowly, as does the average toroidal flux. The line-averaged electron density decays throughout the plasma discharge from 1×10^{19} to 0.5×10^{19} m^{-3}. The central electron and ion temperatures are constant during reference discharges at around 200 eV.

PPCD is fired at $t = 3.5$ ms with a slightly smaller amplitude than in the weak reversal PPCD discharges, resulting in a surface poloidal electric field of ≈ 1.5 V m^{-1}. As shown in figure 7, $\langle B_\phi \rangle$, $B_\phi(a)$ and SXR behave in a manner similar to the weak F PPCD case. A fast change in the equilibrium, characterized by $F = -1.2$ and $\Theta = 2.6$, is then followed by a slower return to the pre-PPCD equilibrium. The line-averaged electron density, contrary to what is observed at weak reversal, does not respond to the PPCD, and the electron density profile is left unchanged by PPCD. It is interesting to note that the plasma current increases during PPCD, a clear sign of a reduction in the plasma resistivity, i.e. an increase in the electron temperature. The increase in the electron temperature has been confirmed with the Thomson scattering system. At the SXR maximum, the shot-averaged electron temperature is about 315 eV and for single discharges it has reached the record value (for EXTRAP T2R) of 380 eV.

Application of PPCD at strong reversal does not always result in a reduction of the magnetic fluctuation level and an increase in the SXR and electron temperature. The reason for this is that sometimes PPCD is fired right after a large sawtooth crash. (For these discharges, the plasma exhibits strong cyclic dynamo activity in the form of large sawtooth crashes.) These discharges are therefore referred to as unsuccessful PPCDs [4]. However, unsuccessful PPCDs do provide interesting information on the ion heating mechanism. As also observed in weak reversal PPCD discharges, the ion temperature is not affected by PPCD, but the $m = 0$ burst terminating the PPCD causes an immediate increase in the ion temperature as shown in figure 8. In particular, for successful PPCD additional energy is stored in the electrons and then, when energy is expelled from the plasma core by the $m = 0$ burst, as testified by the SXR crash, ion heating occurs. For unsuccessful PPCD no electron heating is observed. Instead the ion temperature immediately starts to increase, typically up to 350 eV.
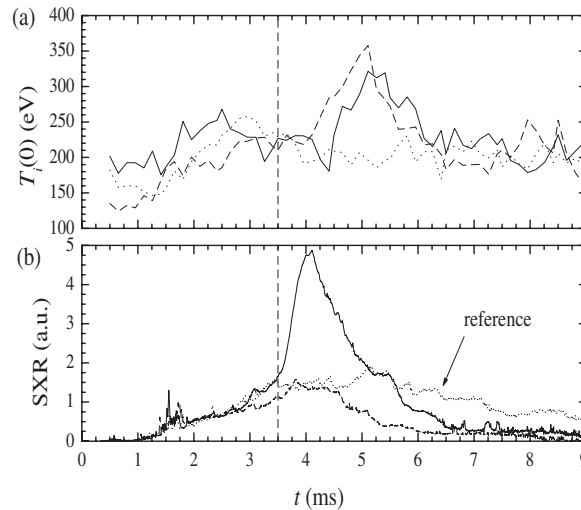

Figure 8. Time evolution of (*a*) the ion temperature and (*b*) the SXR signal for reference discharges (······), successful PPCD discharges (——) and unsuccessful PPCD discharges (- - - -). The vertical dashed line indicates the start of the PPCD.
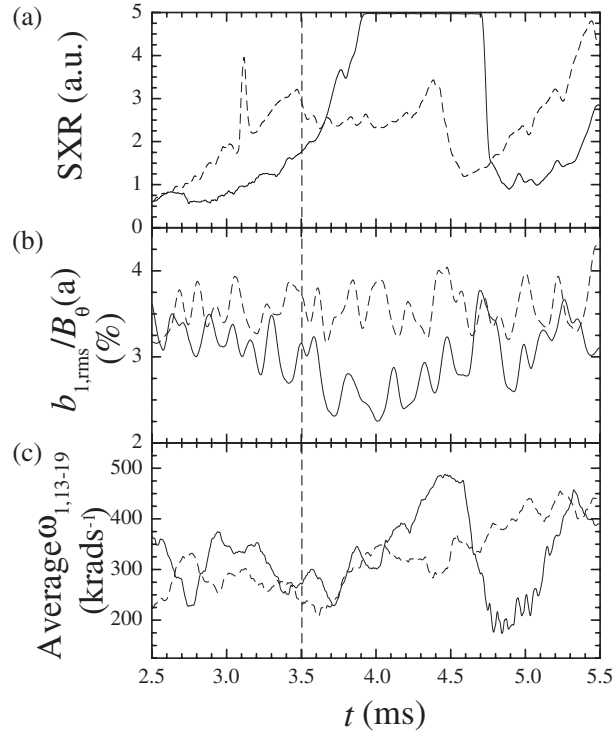
Figure 9. Time traces of a reference (- - - -) and of a PPCD (——) discharge for strong reversal discharges. From top to bottom: (*a*) SXR signal, (*b*) rms value of the $m = 1$, $n = -13$ to -31 internally resonant tearing modes and (*c*) average phase velocity of the $m = 1$, $n = -13$ to -19. The vertical dashed line indicates the start of the PPCD.

In figure 9 the time evolution of the rms amplitude calculated including the $m = 1$, $n = -13$ to -31 internally resonant modes, normalized to the poloidal magnetic field at the edge, is shown both for a reference and a PPCD discharge. Similarly to what was reported in [4], it is possible to observe that the successful PPCD discharge shown in figure 9 is preceded by a spontaneous reduction in the fluctuation level. The reduction of the fluctuation level, from 3.5% to 2.5% during the PPCD phase occurs simultaneously with an increase in the SXR signal and an acceleration of the average angular phase velocity of the $m = 1$ internally resonant tearing modes from -300 to -500 krad s^{-1}. This increase in angular phase velocity of the internally resonant modes is generally observed in the strong reversal PPCD discharges and can be distinguished from the normal angular phase velocity increase observed in the reference discharges. At the end of the PPCD, the fluctuation level of the $m = 1$ modes is restored to that before PPCD. The SXR signal crashes and the $m = 1$ modes rotation velocity decreases to about -200 krad s^{-1}. The reduction in the $m = 1$ fluctuation level is not accompanied by a significant change in the amplitude of the $m = 0$, $n = 1$ mode as shown in figure 10. This is similar to the case of weak reversal. It should be noted that reference discharges are characterized by periodic $m = 0$ bursts (dynamo related), and the rotation frequency of the $m = 0$ modes oscillates in correlation with the occurrence of these bursts. The angular phase velocity of the $m = 0$, $n = 1$ mode is negative at the beginning of the PPCD; it slows down and then reverses direction by the end of the PPCD phase, marked by a SXR crash and an $m = 0$ burst.
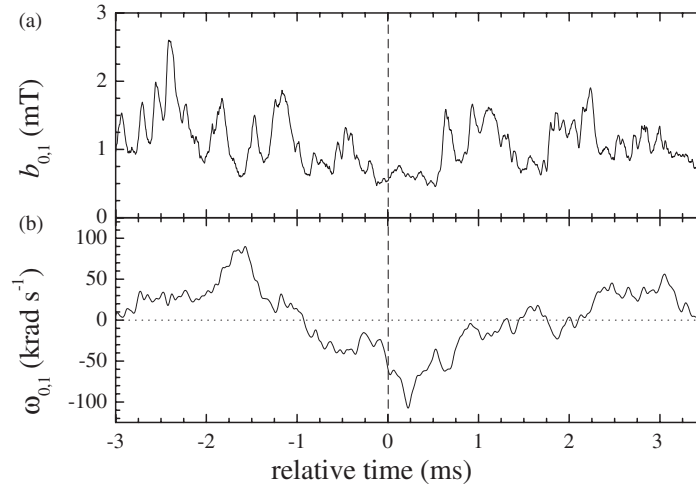
Figure 10. Time traces of (*a*) the amplitude and (*b*) the phase velocity of the $m = 0$ mode for strong reversal discharges with PPCD. Data shown relative to the application of PPCD ($t = 0$ ms). The vertical dashed line indicates the start of the PPCD.
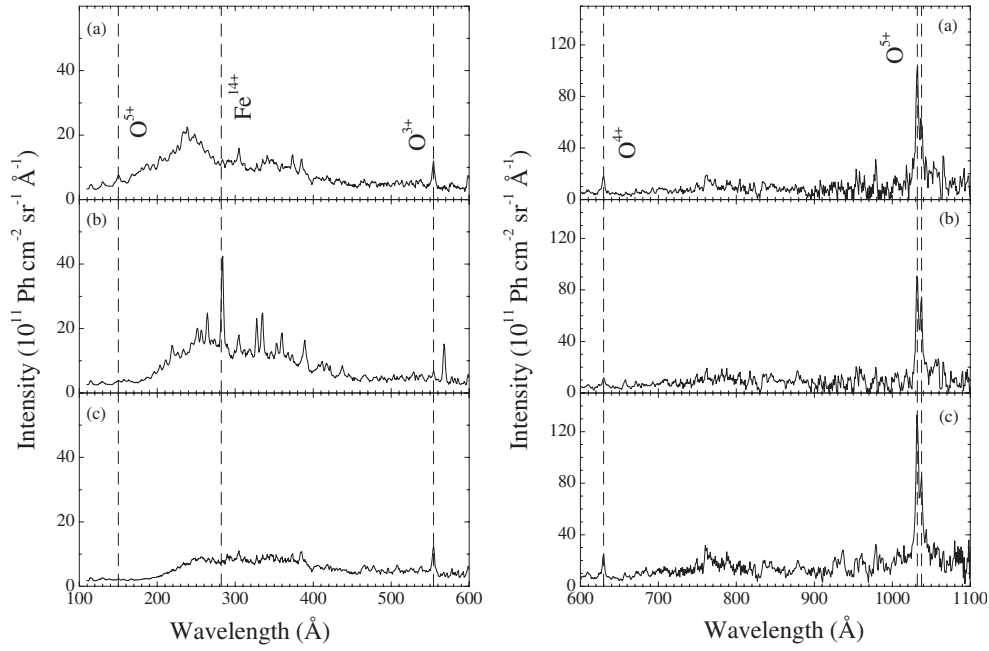

Figure 11. VUV spectrum for a strong reversal PPCD discharge at different times: (*a*) 2 ms, (*b*) 4 ms and (*c*) 6 ms. Indicated in the spectra (with dashed vertical lines) are the spectral lines of O^{3+} (554.3 Å), O^{4+} (629.7 Å), O^{5+} (150.1 and 1032.0–1037.6 Å) and Fe^{14+} (284.2 Å).

3.3. Spectroscopic observations

The temporal evolution of the radiation emitted by impurities has been investigated during PPCD both for weak and strong reversal discharges. Figure 11 shows typical VUV spectra
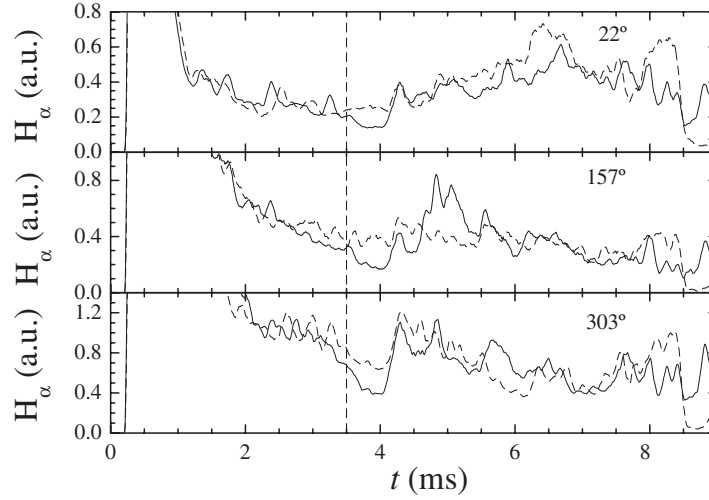
Figure 12. Shot-averaged H_α emission for successful (——) and unsuccessful (- - - -) PPCD at strong reversal at three different toroidal positions, 22°, 157° and 303°. The vertical dashed line indicates the start of the PPCD.

measured before, during and after PPCD in a strongly reversed discharge (similar observations are also made in weak reversal discharges). Indicated (with vertical lines) are spectral lines of O^{3+} (554.3 Å), O^{4+} (629.7 Å), O^{5+} (150.1 and 1032.0–1037.6 Å) and Fe^{14+} (284.2 Å). The strong emission line from Fe^{14+} at 284.2 Å appears after PPCD is fired. The spectra also contain emissions of several spectral lines of Fe^{13+} and Fe^{15+}. The ionization potential for these ionization stages ranges from 392.2 to 489.3 eV. The appearance of these spectral lines indicates a higher central electron temperature during PPCD. After PPCD, the spectral emission at 284.2 Å disappears. The lower ionization stages of iron, which are always present in EXTRAP T2R discharges as a quasi-continuum between 200 and 400 Å, remain present in the spectra.

The VUV spectra show a more complex behaviour in the emission from oxygen, which is the main impurity in EXTRAP T2R plasmas. The emission from lower ionization stages O^{3+} and O^{4+} decreases slightly during PPCD as expected with an increasing electron temperature. After PPCD, their emission increases again, indicating a lower temperature. Spectral emissions from O^{5+} at 150.1 Å and at 1032.0–1037.6 Å behave differently. During PPCD, the emission from O^{5+} at 150.1 Å disappears almost completely while the 1032.0–1037.6 Å multiplet decreases more moderately. This is consistent with an increase in the central electron temperature and a more peaked radial profile [17]. O^{5+} is one of the dominating ionization stages of oxygen and is present over the whole plasma radius. In the hotter interior, O^{5+} moves to the next ionization stage, resulting in a reduction of O^{5+} line emission. In the outer part of the plasma, the electron energy is too low to excite the 150.1 Å transition that requires ≈80 eV. However, it is still sufficient to excite O^{5+} to emit at 1032.0–1037.6 Å, since the excitation energy for this transition is only about 12 eV. The result of the line-integrated intensity is that the 150.1 Å spectral line decreases more strongly than the 1032.0–1037.6 Å multiplet.

The shot-averaged H_α emission at different toroidal positions is shown in figure 12 both for successful and unsuccessful PPCDs discharges at strong reversal. The characteristic burst of H_α associated with sawtooth activity and, in particular, the $m = 0$, $n = 1$ mode burst at the end of PPCD are evident. However, during PPCD the H_α emission for successful PPCDs is

somewhat lower than the H_α emission for unsuccessful PPCDs: this reduction in the H_α signal occurs simultaneously at all three toroidal positions, therefore indicating a reduction in the plasma–wall interactions for successful PPCDs.

Finally, the radiated power, estimated from VUV spectra in the wavelength region between 100 and 1100 Å, shows a decrease during PPCD, similar to observations in RFX [5, 18].

3.4. Confinement properties

The reduction observed in the magnetic fluctuations during PPCD results in an improvement in the plasma confinement properties. This improvement is observed to be more pronounced in PPCD experiments at strongly reversed equilibria. Estimates of the plasma confinement properties are based on pressure and magnetic profile modelling. The electron density profile is modelled according to $n_e(r) = n_e(a) + [n_e(0) - n_e(a)][1 - (r/a)^\alpha]^\gamma$, where the parameters $n_e(0)$, α and γ are obtained by fitting the model to the line-averaged electron density measured along four chords [9]. The ion and electron temperature profiles are not measured in EXTRAP T2R and therefore the following profile is assumed: $T_{i,e}(r) = T_{i,e}(a) + [T_{i,e}(0) - T_{i,e}(a)][1 - (r/a)^\delta]$, where $T_i(0)$ and $T_e(0)$ are measured with the neutral particle energy analyser and the Thomson scattering system, respectively [9]. The ion and electron temperatures at the edge are assumed to be equal to 20 eV [19]. The profile parameter δ has been chosen equal to 4 since this value best reproduces the experimental arrival time distribution function of neutral particles as measured with the neutral particle energy analyser [9]. In the calculations presented here, the profile parameter δ has been kept constant during PPCD both for weak and strong reversal PPCD discharges. This is partly justified by the observation that both the electron density and the SXR emissivity profiles do not change very much in shape during PPCD (as shown in figure 2).

The poloidal and total betas are defined as $\beta_\vartheta = 2\mu_0[\int n_e(T_e + T_i)\,dV / \int dV]/B_\vartheta(a)^2$ and $\beta_{tot} = 2\mu_0[\int n_e(T_e + T_i)\,dV / \int dV]/[B_\vartheta(a)^2 + B_\phi(a)^2]$, respectively, assuming $n_e = n_i$. The total beta is a better indicator of the plasma β for the strongly reversed PPCD discharges since the toroidal magnetic field at the edge is not negligible. The energy confinement time is defined as $\tau_E = W/(P_{inp} - dW/dt)$. W is the plasma kinetic energy defined as $W = \int n_e(T_e + T_i)\,dV$ and P_{inp} is the input power calculated as $P_{inp} = P_{tot} - dU_M/dt$, where P_{tot} is the total input power, calculated by surface integration of the Poynting's vector on the plasma surface, and U_M is the magnetic energy calculated as $U_M = \int (B_\vartheta^2 + B_\phi^2)\,dV/2\mu_0$. The magnetic profiles are modelled according to the α–Θ_0 model [20]. The time derivatives dW/dt and dU_M/dt are calculated by numerical differentiation of W and U_M, respectively. The time evolution of P_{inp}, dW/dt and dU_M/dt during PPCD is shown in figure 13 both for the weak and strong reversal scenarios. The term dW/dt is small compared with the other terms in the power balance equation, and its effect on the energy confinement time is negligible. If a different temperature profile parameter were to be chosen (and kept constant during PPCD) the plasma beta and energy confinement time would change accordingly: if for example δ is set equal to 2, the plasma beta and energy confinement time would decrease by 17% and 19%, respectively.

The time evolution of β_ϑ and τ_E for the weak and strong reversal PPCD scenarios is shown in figure 14. For weak reversal discharges the poloidal beta does not change significantly during PPCD, remaining at $\approx 9\%$. A more substantial improvement is observed for the strong F PPCD discharges in which β_ϑ increases from 10% to 13.5%. The total beta β_{tot} increases from 9% to 11.6%. The energy confinement time increases during PPCD both in the weak and strong reversal cases. For weak F discharges, τ_E increases from 90 to 170 μs. Even though this improvement is significant, similar energy confinement times have been observed in EXTRAP T2R in discharges obtained in different experimental conditions and without
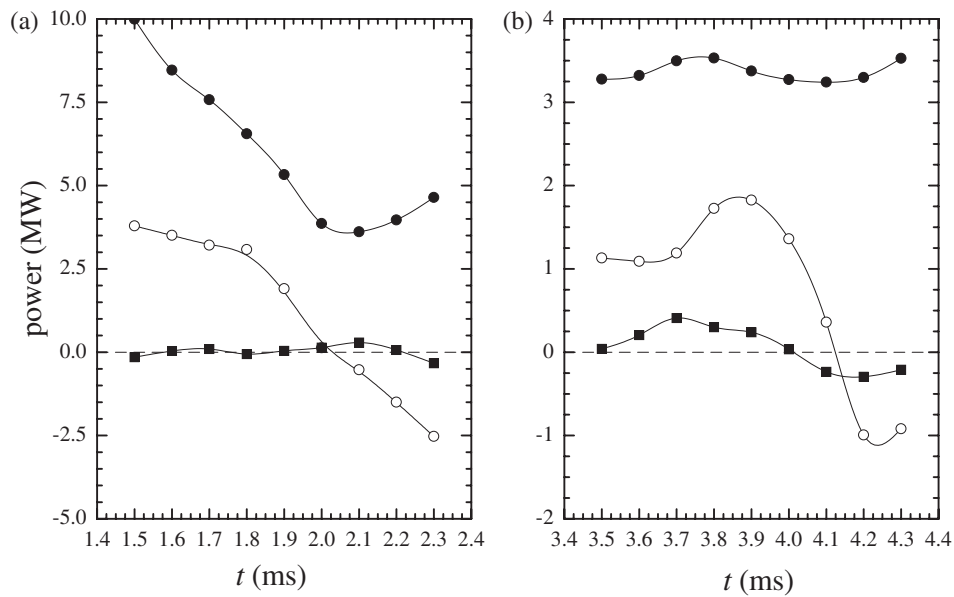
Figure 13. Evolution of the total power (●), the magnetic energy time derivative (○) and the plasma kinetic time derivative (■) for (a) weakly reversed PPCD discharges and (b) strongly reversed PPCD discharges.
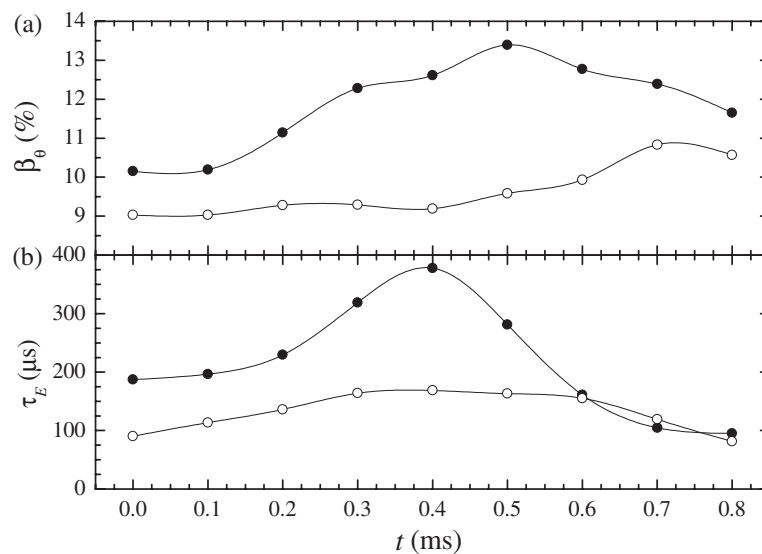

Figure 14. Evolution of (a) the poloidal beta and of (b) the energy confinement time for PPCD discharges at weak (○) and strong (●) reversal. Data shown from the start of the PPCD ($t = 0$ ms).

PPCD [9]. However, an energy confinement up to 380 μs is obtained during PPCD in strongly reversed discharges. In both cases, the confinement improvement is due to a reduction in the estimated input power. This is small for weak reversal discharges (−20%) but quite substantial for strong reversal discharges (−40%). The reduction in the estimated input power is associated

with a hotter and less resistive plasma as confirmed by the measured high electron temperatures and the increase in the plasma current as shown in figure 7. It is however important to stress that estimates of the input power rely on an accurate estimate of the current profiles. The α–Θ_0 model predicts, both for the weak and strong reversal discharges, a peaking of the parallel current density profile with α reaching values as low as 1.5. Similar observations have been reported in [1] and it was speculated that more peaked profiles during PPCD were tolerable at a reduced fluctuation level [21]. The current density profiles obtained with the α–Θ_0 are in agreement with profile reconstruction constrained by experimental measurement (among them that of the magnetic field on axis) [4, 22] and with simulations of PPCD action with three-dimensional MHD resistive non-linear code [23].

Finally, it is observed that the confinement properties of the plasma at the end of PPCD are comparable with those before the PPCD despite the presence of a large SXR crash.

4. Summary and concluding discussion

The magnetic activity during PPCD experiments in EXTRAP T2R shows both similarities and differences with respect to PPCD experiments carried out in other RFPs. The reduction in the fluctuation level of the internally resonant tearing $m = 1$ modes during PPCD operations observed in EXTRAP T2R confirms the effectiveness of current profile modification in substituting the natural dynamo activity. The reduction in the fluctuation level is comparable with what has been observed in the single-pulse PPCD experiments in MST [1, 24] and in TPE-RX [6]. No small $m = 0$ bursts are observed during PPCD, contrary to what was reported in [1]. In addition, no small SXR crashes are observed during PPCD for weak reversal discharges. The enhanced $m = 0$ activity during PPCD, either in the form of small bursts or more continuous, has been associated in MST with PPCD operations beyond a soft density limit and with relatively large applied poloidal electric fields [4]. In EXTRAP T2R, the fluctuation level of the $m = 0$ modes, although not reduced, does not increase during PPCD despite the fact that the line-averaged electron density ($1.5 \times 10^{19}\,\mathrm{m}^{-3}$) is above the density limit observed in MST and that the poloidal electric field at the edge is greater than $1.5\,\mathrm{V\,m}^{-1}$. The change in the equilibrium towards higher Θ values, due to the externally applied poloidal electric field, affects the dynamics of the unstable internally non-resonant resistive shell modes ($n < 0$) in such a way that their growth rates decrease during PPCD.

Spectroscopic measurements confirm the increase in the central electron temperature during the current drive experiments. In particular O^{5+} is burned-through in the plasma core and the Fe^{14+} line at 284.2 Å becomes dominant. This points to a more peaked profile for the electron temperature during PPCD discharges than during reference discharges. Independent confirmation of a hotter plasma core, with temperatures as high as 380 eV, during PPCD operations is provided by Thomson scattering measurements. This is further confirmed by the acceleration of the average angular phase velocity of the $m = 1$ modes.

The reduction in the fluctuation level and the corresponding increase in the energy confinement time are qualitatively consistent with the Rechester–Rosenbluth theory of parallel transport along stochastic magnetic fields lines [25]. The behaviour of the central ion temperature during and after the PPCD seems to indicate that the ion heating mechanism is linked, through magnetic relaxation, to the activity of $m = 0$ modes. The increase in the ion temperature following the $m = 0$ burst at the end of the PPCD, both in weak and strong reversal equilibria, is consistent with observations made in TPE-RX [6].

The PPCD experiments carried out in EXTRAP T2R indicate that a resistive shell does not affect negatively the global improvements in the plasma properties achievable with current profile modification.

Acknowledgments

References

[1] Sarff J S *et al* 1994 *Phys. Rev. Lett.* **72** 3670
[2] Stoneking M R *et al* 1997 *Phys. Plasmas* **4** 1632
[3] Sarff J S *et al* 1997 *Phys. Rev. Lett.* **78** 62
[4] Chapman B E *et al* 2002 *Phys. Plasmas* **9** 2061
[5] Bartiromo R *et al* 1999 *Phys. Rev. Lett.* **82** 1462
[6] Yagi Y *et al* 2002 *Plasma Phys. Control. Fusion* **44** 335
[7] Brunsell P R *et al* 2001 *Plasma Phys. Control. Fusion* **43** 1457
[8] Malmberg J-A and Brunsell P R 2002 *Phys. Plasmas* **9** 212
[9] Cecconello M *et al* 2002 *Plasma Phys. Control. Fusion* **44** 1625
[10] Fonck R J *et al* 1982 *Appl. Opt.* **21** 2115
[11] Klose J Z and Wiese W L 1989 *J. Quant. Spectrosc. Radiat. Transfer* **42** 337
[12] Hedqvist A and Rachlew-Källne E 1998 *Plasma Phys. Control. Fusion* **40** 1597
[13] Franz P *et al* 2002 *High Temperature Plasmas Diagnostics Conf. (Madison)*
[14] Hirano Y *et al* 1996 *Nucl. Fusion* **36** 721
[15] Hender T C *et al* 1989 *Nucl. Fusion* **29** 1279
[16] Brunsell P R *et al* *Phys. Plasmas* at press
[17] Gravestijn R M *et al* 2003 *Proc. 30th European Physical Society Conf. on Controlled Fusion and Plasma Physics (St Petersburg, 7–11 July)* (European Conference Abstracts) vol 27A p-2.71
[18] Carraro L *et al* 2002 *Plasma Phys. Control. Fusion* **44** 2135
[19] Vianello N *et al* 2002 *Plasma Phys. Control. Fusion* **44** 2513
[20] Antoni V *et al* 1986 *Nucl. Fusion* **26** 1711
[21] Stoneking M R *et al* 1997 *Phys. Plasmas* **4** 1632
[22] Brower D L *et al* 2002 *Phys. Rev. Lett.* **88** 185005
[23] Puiatti M E *et al* 2003 *Nucl. Fusion* **43** 1057
[24] Sarff J S *et al* 1995 *Phys. Plasmas* **2** 2440
[25] Rechester A B and Rosenbluth M N 1978 *Phys. Rev. Lett.* **40** 38